High resolution saturated hydraulic conductivity logging of friable to poorly indurated borehole cores using air permeability measurements

Rogiers B.[1,2*], Winters P.[2], Huysmans M.[2,3], Beerten K.[1], Mallants D.[4], Gedeon M.[1], Batelaan O.[2,3,5], Dassargues A.[2,6]

[1] Institute for Environment, Health and Safety, Belgian Nuclear Research Centre (SCK•CEN), Boeretang 200, BE-2400 Mol, Belgium.

[2] Dept. of Earth and Environmental Sciences, KU Leuven, Celestijnenlaan 200e - bus 2410, BE-3001 Heverlee, Belgium.

[3] Dept. of Hydrology and Hydraulic Engineering, Vrije Universiteit Brussel, Pleinlaan 2, BE-1050 Brussels, Belgium.

[4] Groundwater Hydrology Program, CSIRO Land and Water, Waite Road - Gate 4, Glen Osmond SA 5064, Australia.

[5] School of the Environment, Flinders University, GPO Box 2100, Adelaide SA 5001, Australia.

[6] Hydrogeology and Environmental Geology, Dept. of Architecture, Geology, Environment and Civil Engineering (ArGEnCo) and Aquapole, Université de Liège, B.52/3 Sart-Tilman, BE-4000 Liège, Belgium.

* Corresponding author: Bart Rogiers, brogiers@sckcen.be, +32 14 33 31 23

Abstract

Saturated hydraulic conductivity (K_s) is one of the most important parameters determining groundwater flow and contaminant transport in both unsaturated and saturated porous media. This paper investigates the hand-held air permeameter technique for high resolution hydraulic conductivity determination on borehole cores using a spatial resolution of ~0.05 m. We test the suitability of such air permeameter measurements on friable to poorly indurated sediments to improve the spatial prediction of classical laboratory based K_s measurements obtained at a much lower spatial resolution (~2 m). About 368 K_s measurements were made on ~350 m of borehole cores originating from the Campine basin, Northern Belgium, while ~5230 air permeability measurements were performed on the same cores. The heterogeneity in sediments, ranging from sand to clayey sand with distinct clay lenses, resulted in a K_s range of seven orders of magnitude. Cross-validation demonstrated that using air permeameter data as secondary variable and laboratory based K_s measurements as primary variable increased performance from R^2 = 0.35 for ordinary kriging (laboratory K_s only) to R^2 = 0.61 for co-kriging. Due to the large degree of small-scale variability detected by the air permeameter, the spatial granularity in the predicted laboratory K_s also increases drastically. The separate treatment of K_h and K_v revealed considerable anisotropy in certain lithostratigraphical units, while others where clearly isotropic at the sample scale. Air permeameter measurements on borehole cores provide a cost-effective way to improve spatial predictions of traditional laboratory based K_s.

Keywords

Hydraulic properties, geostatistics, cross-validation, Neogene aquifer, Belgium

1. Introduction

Saturated hydraulic conductivity (K_s) is one of the most important parameters determining groundwater flow and contaminant transport in both the unsaturated zone and saturated porous media (*e.g.* Freeze and Cherry 1979). Determining the small-scale variability of this parameter is key to evaluate the appropriateness of effective parameters at the scale of groundwater flow modelling applications, typically several orders of magnitude larger than the measurement scale (*e.g.* Ronayne *et al.* 2010; Huysmans and Dassargues 2009, 2011). Moreover, for stochastic simulations of groundwater flow and even more so for contaminant transport, accurate models on the spatial variability of K_s are much needed (Nilsson *et al.* 2007; de Marsily *et al.* 2005).

Sampling of borehole cores is the most direct way to obtain “hard” small-scale K_s data. It does require expensive minimally disturbed coring, but the obtained data quality is unmatched by other approaches. While several well-established laboratory methods exist for determining K_s, investigating the small-scale variability remains a challenge as it requires collecting large numbers of samples. Indeed, if several hundreds of metres of borehole core have to be hydraulically characterized at the decimetre to centimetre scale, typically several hundreds to thousands of K_s measurements are required, which makes it costly and time-consuming if traditional methods were used. Hence, the commonly achievable spatial resolution obtained with this approach is limited to the metre scale at best (Rasmussen *et al.* 1993; Beerten *et al.*, 2010; Yu *et al.* 2013). To increase spatial granularity in K_s, various geotechnical and wireline geophysical logging tools have been applied for obtaining high resolution characterization of sediment hydrogeological properties, including traditional resistivity and gamma ray logging (*e.g.* Huysmans and Dassargues 2005; Jiang *et al.* 2013), and a range of more advanced methods such as IP and NMR techniques (*e.g.* Slater 2007; Dlubac *et al.* 2013). The so-called "soft" data is then empirically related to "hard" K_s data through various statistical and geostatistical approaches, or by using theoretical models that relate the measured data quantities such as sediment electrical resistivity or gamma-radiation to K_s. While such soft data may be of a high spatial resolution, its usefulness to estimate K_s is often limited because the measured quantities do not relate directly to the sediment properties governing K_s and hence correlate only moderately with K_s. Moreover, support volumes can be very different between the high resolution soft data and the low resolution hard K_s data (typically from several tens to a few thousand cm^3, e.g. Yu *et al.* 2013)

Since the 1960s, air permeameter devices have been increasingly used to characterize sediment properties, including K_s through conversion from air permeability (k_a) measurements (*e.g.* Bradley *et al.* 1972; Welby 1981). With reliable air permeameters becoming available from the late 80's, a fast and effective semi-direct method exists to determine K_s (*e.g.* Chandler *et al.* 1989; Davis *et al.* 1994). As a result, the use of hand-held air permeameter measurements for determining small-scale K_s heterogeneity has been extensively applied, for instance on natural outcrops and accessible sediments (Goggin *et al.* 1988a; Jensen *et al.* 1994; McKinley *et al.* 2004, 2011; Goss and Zlotnik 2007; Rogiers *et al.* 2013a,b), in quarries (Thomas 1998; Huysmans *et al.*, 2008; Possemiers *et al.* 2012), on soils (Kirkham 1947; Loll *et al.* 1999; Iversen *et al.* 2003; Beerten *et al.* 2012), or on borehole cores of indurated sedimentary rocks for reservoir analog and fault zone characterization (Corbeanu *et al.* 2001; Shipton *et al.* 2002; Dinwiddie *et al.* 2006) possibly with automated laboratory setups (*e.g.* Corbett and Jensen 1992; Halvorsen and Hurst 1990; Robertson and McPhee 1990).

Potential disadvantages of such hand-held air permeameter devices are the often operator-dependent seal quality, sensitivity to the saturation degree of the porous medium, as well as sample surface effects such as weathering or irregularities. To avoid effects of weathering and seal quality problems, the development and use of a small drill hole minipermeameter probe has also received considerable attention (Dinwiddie *et al.* 2003, 2006, 2012; Castle *et al.* 2004).

To our best knowledge, the application of such hand-held air permeameters, or similar laboratory setups, directly on borehole cores or slabs taken from cores typically used for geological descriptions has not been reported in the literature for friable to poorly indurated sediments. This method has the potential to achieve in an efficient manner high resolution K_s data on this type of sediments as well, without the need for additional core sampling from the borehole cores. Moreover, air permeability measurements require times on the order of seconds to minutes, which is only a fraction of the time needed for a constant head test. In principle, the proposed methodology is applicable to any kind of sediment, but excessively long measurement times limit practical applications for very low K_s values (from several minutes up to half an hour for K_s values between 10^{-7} and 10^{-10} m/s). Also, sediment pore diameter should not have a similar scale as the air permeameter probe opening (9 mm in our case), which limits application in gravels. The sediments studied here are friable to poorly indurated fine- to coarse-grained sands with a varying clay content.

This paper therefore investigates the usefulness of the hand-held air permeameter technique for high resolution characterization of K_s on borehole cores. The objectives of this work are i) to test the suitability of the hand-held air permeameter technique for high resolution hydraulic conductivity determination on borehole cores using a spatial resolution of ~0.05 m, ii) to validate and calibrate the obtained data with classical laboratory based K_s measurements, and iii) to quantify the gain in spatial prediction of K_s by using such high resolution air permeameter measurements in combination with laboratory based K_s measurements obtained at a much lower spatial resolution (~2 m).

2. Materials and methods

2.1. Retrieval of borehole cores

As a case study, we use approximately 350 m of borehole cores (Table 1) originating from the Mol/Dessel area in the Campine basin, Northern Belgium (Figure 1). The studied sediments are of Miocene to Pleistocene age, with a marine to continental origin, and consist of poorly indurated sand to clayey sand with distinct clay lenses, resulting in a K_s range of seven orders of magnitude (Beerten *et al.* 2010). During previous studies, two samples were taken from borehole cores every two meters for performing constant head laboratory permeameter tests (Beerten *et al.* 2010; Figure 2c). This hard data is now used as a reference for the secondary information obtained from the air permeameter measurements, performed with a resolution of five centimetres.

Table 1: Overview of the cored sections and number of samples of the different boreholes (Beerten *et al.,* 2010). 100 cm³ steel ring core samples indicated with a star (numbers in parentheses) are located more than 20 cm away from the nearest air permeability measurement. K_h: horizontal hydraulic conductivity; K_v: vertical hydraulic conductivity; k_a: air permeability.

Borehole	Drilling	Cored section (m)	# 100 cm³ K_h	# 100 cm³ K_v	# k_a
Dessel-2	2002	50	38(1*)	46	835
Dessel-3	2008	47	21(3*)	23(1*)	779
Dessel-4	2008	40	17(6*)	21	640
Geel-1	2008	45	21(2*)	23(3*)	794
Kasterlee-1	2008	46	17(6*)	23	709
Retie-1	2008	47	20(6*)	23(2*)	770
Retie-2	2008	41	18(5*)	21(1*)	703
Total		316	152(29*)	180(7*)	5230

** samples not within 20 cm distance of a k_a measurement*

The borehole cores studied in this paper originate from two site characterizations carried out in the framework of the ONDRAF/NIRAS low-level radioactive waste disposal research programme (ONDRAF/NIRAS 2010). A 50-m long borehole core (named Dessel-2) was obtained in the first characterization in 2002 (Mallants *et al.* 2003) aimed at a detailed local study of all relevant lithostratigraphical layers. In total, 50 cores were taken with a push corer in 96 mm-diameter PVC tubes of 1-1.1 m length, resulting in minimally disturbed core samples, which normally result in a high core recovery (Beerten *et al.* 2010). The push corer technology is similar to direct push core sampling (Dietrich and Leven 2006), but used in combination with drilling to be able to achieve larger depths. The intactness of the cores in Figure 3 also illustrates the minimal disturbance of the sediment. Because of the sandy character of all the sediments, the disturbance that potentially did take place happened at the outer section of the cores, while the center of the core is practically unaffected. In some cases the thin plastic clay lenses were slightly deformed at the core perimeter by the pushing. As the sampling and measurements always took place in the center of the core sections, the effect of core disturbance on the results is thought to be minimal. Uncertainties about subsurface knowledge were identified through groundwater flow and contaminant transport modelling studies including sensitivity analyses (Gedeon and Mallants 2009; Gedeon *et al.* 2013). To reduce the uncertainties, a second site characterization was performed in 2008 in an area of ~16 km^2, including six more cored boreholes (266 cores) down to a depth of 40-50 m using the same coring methodology, labelled as Dessel-3, Dessel-4, Geel-1, Kasterlee-1, Retie-1 and Retie-2 (Beerten *et al.* 2010).

Upon receiving the cores in the laboratory, core handling started by sawing the cores longitudinally in a one-to-three proportion with a wire saw (Figure 2a,b). The thinnest slab was used for geological description and air permeability measurements (carried out in 2012), while the main core section was used for further sampling with 100 cm^3 steel rings (5 cm diameter, 5 cm height; Figure 2c) for laboratory K_s measurement. Finally, the cores were vacuum packed in PE-Al film awaiting future analysis.

A typical approximately 1 m-long core section is shown in Figure 3 for each lithostratigraphical unit. The Quaternary unit (Figure 3a) consists mainly of medium dense to loose, fine-grained aeolian sands with organic material and some soil development (Beerten *et al.* 2012). The Mol Upper Sands (Figure 3b) are medium dense, medium to coarse-grained, white, pure quartz sands; the Mol Lower Sands (Figure 3c) belong to the same formation, are well sorted, dense, fine-grained sand and do not contain the very coarse fraction typical of the Mol Upper Sands. The dense Kasterlee Sands (Figure 3d) show a higher fines content (both in the clay and silt fractions), and some presence of the typically green-coloured mineral glauconite (up to one weight %). The main aquitard in the study area is the Kasterlee Clay (Figure 3e), which is a heterogeneous alternation of medium to dense, fine-grained silty or clayey sand layers and clay lenses. Given the large small-scale heterogeneity within this unit, small differences in the vertical position of air permeameter measurements and the corresponding steel ring core samples might induce large differences between the matched data points. This is especially true given the time between the two core characterization campaigns, and we believe that our results would only improve if steel ring core sampling and air permeameter measurements are performed in a single campaign. The upper part of the Diest Formation, the dense Diest Clayey Top (Figure 3f) also has an increased fines content, and the dense Diest Sands (Figure 3g) are medium to coarse-grained glauconite-bearing sands (up to 30 weight %) with typical bioturbation structures (white spots in Figure 3g). The grain size characteristics of these sediments are discussed by Rogiers *et al.*

(2012). Most boreholes contain all lithostratigraphical units; only in a few cases, the Diest Sands were not penetrated at the bottom of the borehole.

Handling of the cores of the most friable sediments therefore had to be performed with caution. The increased cohesion of the wet sediment was an advantage during the sawing of the saturated cores, but minor effects of deformation might be present. Deformation by the air permeameter tip was however only an issue in the most loose sands, only present in a few cores, and care was taken not to put to much pressure on the sediment to avoid deformation as much as possible. The sand and clay retrieved from deeper in the subsurface was compact and well consolidated, and the retrieval of undisturbed cores did not present a problem. Especially the Mol Lower unit was hard to disturb with the air permeameter measurements or core handling. Even intentional manual deformation of this sediment is not easily achievable, and the occasional breaking of steel rods during the direct push campaigns in the area were always due to this unit. Places where deformation did occur during core handling were easily identifiable by *e.g.* small cracks in the sediment, and where omitted during the measurements; missing parts of the most shallow cores were obviously not available for measurement.

2.2. Saturated hydraulic conductivity measurements

Sampling of the main core sections for determination of K_s was performed with 100 cm³ steel rings (Figure 2c). The rings were inserted with the cutting edge down by pushing it manually in the sediment. Once completely inserted, a slight twist was given to the ring to effectively break the bottom plane of the sample, and the sample could be withdrawn intactly from the main core. For characterizing both horizontal (K_h) and vertical (K_v) conductivity at the 100 cm³-scale, a horizontally and vertically oriented sample was taken at each sampling depth at a separation distance of approximately 10 cm. In total 368 samples were retrieved (see Table 1) and K_s was measured in the laboratory using an Eijkelkamp constant-head permeameter (ISO/TS 17892-11 standard; see *e.g.* Klute 1965) and making use of Darcy's law (Darcy 1856). For the most clay-rich samples, a permeameter cell adapted to medium to low K-values (10^{-9} to 10^{-13} m/s) was used (Wemaere *et al.* 2002, 2008). In this setup, water is injected at the bottom of the sample under a constant pressure of about 6 bar. The hydraulic conductivity value is determined only after saturation of the sample, and when a steady flow out of the sample is reached. The precision of the measurements is about 8%.

The investigation of intrinsic sample-scale anisotropy, *i.e.* based on the individual K_h/K_v ratios, using statistical t- and F-tests (Sheskin 2004) in comparing both K_h and K_v datasets, is reported by Beerten *et al.* (2010). Scatterplots of the paired K_h – K_v data are shown in Figure 4. The F-tests are performed for checking the two-tailed probability that the variances are not significantly different, while the t-tests checks the equality of the sample means for a two-tailed distribution and equal or unequal variances depending on the corresponding F-test outcome. The only significantly (at the 0.05 level) different means and variances of the K_h and K_v data, revealed by the t- and F-tests, were those for the lower aquifer data (Diest Clayey Top and Diest Sands). There is however no strong correlation between the K_h and K_v pairs in Figure 4c, and many pairs display larger K_v than K_h. This again indicates the likely importance of the small-scale variability. Because of the distance between the K_h and K_v samples, the apparent absence of isotropy in K_s might be due to small-scale variability induced by the method of sampling. The data points in Figure 4a and b are distributed more or less equally around the 1:1 line (K_h/K_v = 1), likely illustrating considerable spatial variability over short distances which might overprint the existing intrinsic anisotropy. It cannot be confirmed that the laboratory based K_s values are isotropic at the sample-scale, despite the fact that the upper aquifer and aquitard marginal distributions show no significant differences in mean and variance between K_h and K_v. Therefore, all further analyses are done on the K_h and K_v datasets separately.

2.3. Air permeability

A probe permeameter basically consists of an annulus through which gas can be injected in or withdrawn from a porous medium. To prevent leakage between the annulus and the porous medium, compressible impermeable material has to be used at the probe tip. The gas pressure and flow rate should be monitored in order to derive gas permeability by *e.g.* the modified form of Darcy's law including a geometric factor, as proposed by Goggin *et al.* (1988a,b).

A Tinyperm II air permeameter device (New England Research and Vindum Engineering 2011; Figure 2d) was used for the borehole cores in this paper; several successful studies were previously performed using the same device (Huysmans *et al.* 2008; Possemiers *et al.* 2012; Rogiers *et al.* 2013a, b), and extensive testing and comparison with other gas permeameters was performed by Filomena *et al.* (2014). This device consists of a vacuum cylinder, pressure transducer, handle and plunger, and a microprocessor and control unit. The flexible rubber permeameter tip is pressed against the borehole core material, and the plunger is depressed to create a vacuum causing air to flow from the unsaturated porous medium into the device where the gas flow rate and pressure are monitored by the pressure transducer and analysed by the microprocessor unit. Using signal processing algorithms, the unsteady state response function of this transient pressure test is computed and related to the sample k_a. The exact value of k_a can be determined by an equipment specific calibration curve (New England Research and Vindum Engineering 2011). The effective sealing during the measurement was achieved by putting some pressure on the device, and preparing a very flat surface on the core material prior to the measurement (if the core surface wasn't already very smooth). Highly anomalous values, where clearly leakage of air between the rubber nozzle of the air permeameter and the sediment occurred, where discarded when encountered during the borehole core slab measurements, and repeated. To prevent loose sand debris being sucked into the device, a custom made metallic screen was fitted at the outlet. This required recalibration of the TinyPerm II device to correct for modifications to the air flow (Huysmans *et al.* 2008).

The volume of sediment involved in a permeameter measurement for isotropic porous media is often defined by a hemisphere two to four times the internal radius of the tip seal (Goggin *et al.* 1988a; Jensen *et al.* 1994). More recent analyses identified the possible existence of a blind spot (Tartakovsky *et al.* 2000), but this was disproven again by Moltz *et al.* (2003) who accurately determined and quantified the geometry of the flow lines and the spatial weighting function for the conventional surface-sealing mini-permeameter probe. These authors clearly illustrated that the region near the inlet edge of the seal is heavily weighted. The TinyPerm II has an inner tip diameter of 9 mm, and an outer diameter of 21 mm, resulting in an investigation depth of ~11 mm for 95% of the spatial weighting function, and ~19 mm for 99%. These investigation depths are small enough for performing reliable measurements on the core slabs that have a maximum material depth of ~30 mm. Measurements in permeable sands typically take a few seconds, less permeable samples take up to a few minutes and clays might take several dozens of minutes. The by the manufacturer reported measurement range of the device is from 10 mD to 10 D. The lowest value corresponds to a measurement time of ~5 minutes (Filomena *et al.* 2014), but in laboratory conditions measurement times can easily be longer using the handheld approach (up to half an hour in this study), and even up to several hours with a special laboratory setup, as demonstrated by Filomena *et al.* (2014). These authors also tested the technical tightness of the device, which revealed 0.034 mD as an absolute lower boundary. Rogiers *et al.* (2013b) validated a range between ~12 mD and ~60 D on outcrop sediments with the same 100 cm³ steel ring samples as used in this study.

Because totally dry sediment conditions are hard to obtain, especially under field conditions, and because of the polar characteristics of water and gas slippage effects, empirical equations have to be used to convert the obtained k_a values into K_s estimates; from hereon denoted as $K_{s,ap}$. The empirical equation proposed by Loll *et al.* (1999) is used in this study for the initial k_a-based K_s estimates:

$$K_{s,ap} = \frac{10^{1.27\times\log_{10}(k_a\times 9.86923e^{-16})+14.11}}{86400} \quad [1]$$

where k_a is expressed in mD, and $K_{s,ap}$ in m/s. This equation is derived based on the analysis of k_a – K_s relationships for nine soils, six different soil treatments and three horizons, resulting in a dataset of 1614 undisturbed 100 cm³ core samples, and displays a general prediction accuracy better than ~0.7 orders of magnitude. In a recent study on the effect of anisotropy on *in situ* air permeability measurements, Chief *et al.* (2008) indicated that anisotropy might introduce errors as high as a factor of 2 in air permeability estimates. This is so because air flow lines have different directions in the sediment, and the derived k_a value is somewhere in between the true k_h and k_v parameters. Therefore, we use the air permeameter measurements as secondary data for both the K_h and K_v variables in this study, without making assumptions on the k_a anisotropy or the direction of air flow.

On all 316 approximately 1-m long borehole core slabs k_a measurements were carried out with a spacing of approximately 5 cm, resulting in 5230 k_a values. All measurements were performed within 5 days, with one person for handling the air permeameter, and another one to log the Tinyperm II responses.

2.4. Quantification of measurement error and influence of moisture content

Next to the measurements on the core slabs, several additional investigations were performed to better capture the characteristics of the air permeameter device and its limitations. In a first step, the measurement error was quantified by doing 20-30 repeated measurements on each lithology resulting in 280 measurements in total. A second test was designed to investigate the representativity of the core slabs, and the influence of the moisture content on the obtained $K_{s,ap}$ values. For this, we unpacked 12 of the main cores and separated sections of 30 cm for k_a and gravimetric moisture content measurement. Both properties were measured three times: 1) immediately after unpacking, 2) after drying in air during a week, and 3) after 2 additional days of drying in the oven at 100°C, resulting in a total of 171 measurements.

2.5. Calibration of air permeability-based hydraulic conductivity estimates

All K_s values from the laboratory constant head tests on the 100 cm³ steel ring samples were paired with the closest $K_{s,ap}$ values (within a maximum distance of 20 cm) to perform a calibration of the detailed high-resolution $K_{s,ap}$ logs. After considering the equation of Loll *et al.* (1999), a site-specific calibration was tested as a means to increase reliability on $K_{s,ap}$. Moreover, preliminary analysis indicated that the calibration would benefit from including lithostratigraphy as a separate factor in the regression analysis, because different units showed slightly different k_a – K_s relationships. Furthermore, a slight bias was observed between the $K_{s,ap}$ values from the Dessel-2 cores (collected in 2002) and all other cores (collected in 2008); in other words, air permeability measurements were carried out on respectively ten and four year old material. Therefore, we extended the linear model approach with categorical covariates and used a linear mixed-effects model (McLean 1991) with random effects for both the stratigraphy and borehole factors. This allows for different linear relationships for different boreholes and stratigraphical layers, while accounting for the general relationship between K_s and $K_{s,ap}$. This was done for K_h and K_v treated separately as predictor variables. The models were fitted with the lme4 package (Bates *et al.* 2012) developed in the R language (R Development Core Team, 2012).

2.6. Geostatistical analysis

After calibration of the high-resolution $K_{s,ap}$ data, a geostatistical analysis was performed to provide the best possible estimates (i.e. spatially interpolated) of the primary K_s data by invoking the spatially cross-correlated secondary $K_{s,ap}$ data. This analysis consisted of the following steps: 1) experimental variography for the primary and secondary datasets after standardization of the data, 2) fitting of direct variograms and cross-variograms using an intrinsic model of co-regionalization (Goovaerts 1997), 3) interpolation by co-kriging, and 4) perform a leave-one-out cross-validation to quantify the predictive uncertainty on K_s (kriging variance), as well as the gain in accuracy (performance of the spatial interpolation model) by using the correlated secondary data. These steps were implemented twice, once for the K_h dataset and once for the K_v dataset. All analyses were performed within R, making extensive use of the gstat package (Pebesma 2004).

3. Results and discussion

All raw data encompassing the 100 cm³ steel ring core sample data and the $K_{s,ap}$ values obtained from the equation of Loll *et al.* (1999) are shown in Figures 5 and 6. Especially in the clay-rich units (Kasterlee Clay, Diest Clayey Top) there is a clear mismatch between the laboratory-derived and the air permeameter-based values, while in the sand-dominated units a good match is observed. The sand-dominated units were all dry during measurement allowing for reliable estimation of K_s through $K_{s,ap}$; presence of clay generally results in less reliable measurements (measurements may not have reached equilibrium, while microscopic fissures in the dried clay may yield overestimations) which may have caused the discrepancies in the clay-rich units. Nevertheless, the differences are not as large as the systematic bias observed by Rogiers *et al.* (2013c), when comparing outcrop air permeameter data to these borehole core laboratory-derived K_s values.

Boxplots for the laboratory-derived K_s values, and the initial $K_{s,ap}$ estimates derived from the equation of Loll *et al.* (1999) are shown in Figure 6. For a given measurement type (K_h, K_v, or $K_{s,ap}$) the relative differences between the different units seem to be honoured, but the absolute mean K_s values differ significantly from $K_{s,ap}$ for all cases except the Diest Sands K_h. Such discrepancies were not observed when air permeability measurements on outcrop sediments were compared with lab-based K_s values on 100 cm³ steel ring samples of the same outcrops (Rogiers *et al.* 2013b). Factors that may have contributed to the discrepancies include borehole core slabs that have been subject to drying in open air and displacement of slabs rendering certain sections in a disturbed condition, thus causing a systematic bias towards higher $K_{s,ap}$ values. Moreover, the air permeameter data show a considerably higher number of values outside of the 95% confidence interval; this might be due in part to the much larger data set compared to the lab-based data (~14 times), and the smaller support volume of the air permeameter measurements (between 2.8 cm³ for 95% of the spatial weighting function of Molz *et al.* (2003) and 14 cm^3 for 99%) compared to the 100 cm³ steel ring samples.

The measurement error, including the intrinsic variability in response of the device as well as operator-dependent influence (way of handling the plunger or pressure applied on the rubber tip for sealing), was investigated by doing repeated measurements. The results indicated that the measurement error variance of maximum 0.017 (in terms of logarithmic $K_{s,ap}$) clearly is small compared to the variability within a single lithostratigraphical unit (Figure 6). The operator influence also shows a relatively small effect, but it is clearly present. The bias between the two operators reached a maximum of 0.16 for the tested clayey sample, but was always below 0.08 for the sandy samples (again in terms of logarithmic $K_{s,ap}$). It thus seems to be more important for lower $K_{s,ap}$ values.

The air permeameter measurements at different times during the drying (*i.e.* decreasing gravimetric water content) of the full-sized cores are shown in Figure 7. Water content clearly has an important effect on $K_{s,ap}$ values, through the availability of pores of different sizes for air flow, which depends on the sediment texture and structure. For instance, water content changes of a few percent can lead to changes of up to an order of magnitude for the clayey samples, as the largest pores or cracks will first be available for air flow. For the sand-dominated units the effect on $K_{s,ap}$ is small: most values remain within one order of magnitude difference considering a water content range from 16 to zero %. Note however that differences in $K_{s,ap}$ due to water content changes of a few percent are of comparable magnitude as the measurement error (0.10 for $\log_{10}(K_{s,ap})$). Because all measurements were performed in the same dry conditions, *i.e.* dried in air at room temperature for several years, effects (and bias) within the same unit are similar. Because the $K_{s,ap}$ values are only used as secondary data after calibration with lab-based K_s, effects of water content become unimportant, recognizing though that the degree of correlation between primary and secondary data may depend on water content.

The predictive capacity of the equation of Loll *et al.* (1999) to generate reliable K_s estimates is demonstrated in Figure 8a. The scatterplot shows that values derived for the predominantly sandy sediments have the correct order of magnitude, while the very low $K_{s,ap}$ pertaining to Kasterlee Clay clearly shows a systematic bias of two to three orders of magnitude. Overprediction of K_s, using the air permeameter $K_{s,ap}$ values for the clayey sediments is likely due to modifications of the pore structure after a long period of drying (opening of cracks), also recognizing that the very low K_s values are probably beyond the measurement range of the Tinyperm II, and that an inherent variability is introduced by not having air permeameter and laboratory measurements at the same locations. The R^2 based on the combined data set (K_h and K_v) is 0.50, but depends on the maximum distance used for matching laboratory based and air permeameter measurements (*e.g.* using 10 cm rather than 20 cm as maximum distance results in an R^2=0.55). The predictive capacity of the $K_{s,ap}$ data can be significantly improved through calibration. Using linear mixed effect models for the K_h and K_v data increases the R^2 to 0.72 (Figure 8b).

After standardization of both the laboratory and calibrated air permeameter data (using the linear mixed effects models for K_h and K_v), experimental variograms were calculated for the entire dataset (Figure 9), assuming similar spatial variability at the different boreholes. As the data shows considerable scatter within lag distances less than 0.4 m, we decided to extrapolate the semivariance at 0.4 m to a nugget value of zero at the origin, using a spherical model with a 0.4 m range. The increase of the semivariance between 0.4 and 20 m was captured by adding a second spherical model with a range of 12 m. The only differences between the K_h and K_v variogram models are the partial sills, with the K_v model showing the higher semivariance at short distances.

For determining the cross-variograms between laboratory K_s and $K_{s,ap}$, we multiplied the partial sills of the direct variogram models with the respective correlation coefficients for K_h (0.88) and for K_v (0.82). This approach is more robust than using the experimental cross-variogram, given the limited amount of primary data (368) in comparison with the secondary data (5230).

The best K_h and K_v estimates for each 2 cm along the borehole core sections were then determined using co-kriging with the laboratory data as primary variable and the air permeameter data as secondary data. The results for K_h are displayed in Figure 10, together with the 95% confidence intervals (based on the kriging variance). The largest uncertainties are located in the zones where core slabs were missing, and hence no secondary data is available.

Nearly continuous estimates of K_s are obtained in this way, revealing a lot more heterogeneity of the subsurface than the lab-based K_s dataset only. Especially the structure of the Kasterlee Clay displays a high degree of heterogeneity at each borehole location, with several discrete clay lenses sandwiched in-between coarse-grained sand layers. A few other thin lenses with finer material are revealed as well and occur outside of the current boundaries of the Kasterlee Clay unit. Such information could be used to revise the location of several litho-stratigraphical boundaries. Compared to all other boreholes, the Dessel-2 borehole shows more scatter in the data, which could be attributed to the longer exposure of the core slabs to air compared to the 2008 cores.

To investigate the intrinsic anisotropy at the measurement scale of 100 cm^3 after the secondary k_a data has been accounted for, the co-kriging estimates for both K_h and K_v are shown in Figure 11. The results indicate that mainly the lower aquifer sediments and several parts of the Mol Lower and

Kasterlee Sands show systematic intrinsic sample-scale anisotropy, as was previously indicated by the statistical t- and F-tests. The Mol Upper Sands are consistently isotropic, except for the upper part in the Dessel-2 borehole.

Validation of the use of calibrated k_a as secondary variable in a co-kriging approach with lab-based K_s as primary variable and the derived variogram models, was done on the basis of leave-one-out cross-validation (see Table 2 and Figure 12). Ordinary kriging and ordinary co-kriging was compared for all cases (once for all K_h and once for all K_v samples) to quantify the benefit of using $K_{s,ap}$ as secondary variable for spatial interpolation of K_s. Inverse distance weighting as an alternative interpolation technique was also performed to quantify the benefit of accounting for data-based spatial variability.

According to all performance measures in Table 2, the ordinary co-kriging approach with the secondary air permeameter data performs best as spatial interpolation technique for the lab-based K_s measurements. The main gain in performance is for the clayey samples which occur mainly in the more heterogeneous parts and which are more difficult to predict based on the primary dataset only. Given the large amount of small-scale heterogeneity, the difference in performance between the inverse-distance weighting and ordinary kriging is small.

Table 2: Leave-one-out cross-validation results. IDW: inverse distance weighting; OK: ordinary kriging; OCK: ordinary co-kriging; MSE: mean squared error; MAE: mean absolute error; ME: mean error; ρ: correlation coefficient; R²: coefficient of determination; NSeff: Nash-Sutcliffe efficiency.

Performance measure	IDW	OK	OCK
MSE	1.20	1.04	0.68
MAE	0.73	0.68	0.59
ME	0.05	0.02	0.02
ρ	0.56	0.59	0.78
R^2	0.31	0.35	0.61
NSeff	-0.06	-0.25	0.57

4. Conclusions

A hand-held air permeameter was used to obtain high-resolution information on K_s variability from borehole core slabs of friable to poorly indurated sands to clayey sands with distinct clay lenses. Calibration with independent lab-based K_s measurements improved the predictive capacity of the Loll et al. (1999) equation considerably and resulted in more reliable $K_{s,ap}$ values. The regression model for lab-based K_h measurements with linear mixed effects gave the overall best result. Based on a 5-cm measurement interval, the air permeability based $K_{s,ap}$ values revealed considerable small-scale spatial variability, with an overall range between 10^{-10} and 10^{-3} m/s. The measurement error was quantified, as well as the influence of the operator, and both proved to be small compared to the $K_{s,ap}$ variability.

Spatial interpolation using the site-specific air permeability calibration with linear mixed effects models as secondary variable in an ordinary co-kriging approach proved to be reasonably accurate based on a full leave-one-out cross-validation with an R^2 of 0.61. In comparison, an R^2 of 0.31 and 0.35 was obtained for respectively inverse distance weighting and ordinary kriging. Especially the interpolated K_s estimates of the thin clay lenses improved drastically. Finally, a comparison of the interpolated high-resolution K_h and K_v profiles revealed that at the 100 cm^3 sample scale anisotropy is obvious in certain lithostratigraphical units, which was not evident from an analysis of the primary lab-based K_s dataset alone.

The presented analyses were performed for the K_h and K_v datasets separately. Accounting for the correlation between both variables would improve the accuracy of the methodology, but is not straightforward with large small-scale variability and the lack of co-located (at least in vertical direction) samples.

The obtained high-resolution data can potentially be used as a reference for correlating more easily gathered direct push data like cone penetration tests with K_s in order to be able to make regional data-conditioned stochastic realizations of shallow aquifers accounting for small-scale variability (Rogiers *et al.* 2014). Moreover, in the framework of monitoring network design, such high resolution data allow for the optimal placement of multi-level monitoring wells.

In conclusion, the hand-held air permeameter is an efficient cost-effective tool to obtain high-resolution information on K_s and its variability from borehole core slabs. While such measurements are used regularly in lithified sediments in the framework of studying fault rocks and reservoir analogues, we demonstrated that this approach can equally well work for friable to poorly indurated sands and clays.

Acknowledgements

Serge Labat and Frans Slegers are acknowledged for their help with handling the borehole cores. The authors further wish to acknowledge the Fund for Scientific Research – Flanders for providing a Postdoctoral Fellowship to Marijke Huysmans, and the associate editor and two reviewers for their constructive comments on an earlier version of this manuscript. ONDRAF/NIRAS, the Belgian Agency for Radioactive Waste and Enriched Fissile Materials, is acknowledged for granting access to the borehole cores and providing the laboratory data. Findings and conclusions in this paper are those of the authors and do not necessarily represent the official position of ONDRAF/NIRAS.

References

Bates D, Maechler M, Bolker B (2012) lme4: Linear mixed-effects models using S4 classes. R package version 0.999999-0. http://CRAN.R-project.org/package=lme4

Beerten K, Wemaere I, Gedeon M, Labat S, Rogiers B, Mallants D, Salah S, Leterme B (2010) Geological, hydrogeological and hydrological data for the Dessel disposal site. Project near surface disposal of category A waste at Dessel – Version 1.- Brussels, Belgium: NIRAS/ONDRAF, 2010.- 273 p.- NIROND–TR 2009–05 E V1. Available from www.researchgate.net/publication/248707737, last accessed on 22/01/2014.

Beerten K, Deforce K, Mallants D (2012) Landscape evolution and changes in soil hydraulic properties at the decadal, centennial and millennial scale: A case study from the Campine area, northern Belgium. Catena 95: 73-84

Bradley VW, Duschatko RW, Hinch HH (1972) Pocket permeameter: Handheld device for rapid measurement of permeability: Bull. Am. Association Petroleum Geologists 56: 568-571

Castle JW, Molz FJ, Lu S, Dinwiddie CL (2004) Sedimentology and fractal-based analysis of permeability data, John Henry Member, Straight Cliffs Formation (Upper Cretaceous), Utah, U.S.A. Journal of Sedimentary Research 74(2): 270–284

Chandler MA, Goggin DJ, Lake LW (1989) A mechanical field permeameter for making rapid, non-destructive permeability measurements. J Sediment Petrology 59(4): 613-635

Chief K, Ferré TP, Hinnell AC (2008) The effects of anisotropy on in situ air permeability measurements. Vadose Zone J 7(3) : 941. doi:10.2136/vzj2007.0164

Corbeanu RM, Soegaard K, Szerbiak RB, Thurmond JB, McMechan GA, Wang D, Snelgrove S, Forster CB, Menitove A (2001) Detailed internal architecture of a fluvial channel sandstone determined from outcrop, cores, and 3-D ground-penetrating radar: Example from the middle Cretaceous Ferron Sandstone, east-central Utah. AAPG Bulletin, 85(9), 1583–1608.

Corbett PWM, Jensen JL (1992) Variation of reservoir statistics according to sample spacing and measurement type for some intervals in the lower Brent Group. Log Analyst 33: 22–41

Darcy H (1856) Les Fontaines Publiques de la Ville de Dijon Dalmont Paris. 647 p.

Davis JM, Wilson JL, Phillips FM (1994) A portable air-minipermeameter for rapid in situ field measurements. Ground Water 32(2): 258–266

De Marsily G, Delay F, Goncalves J, Renard Ph, Teles V, Violette S (2005) Dealing with spatial heterogeneity. Hydrogeology J: 13(1) 161–183

Dietrich P, Leven C (2006) Direct push-technologies. In Kirsch R (Ed.), Groundwater geophysics, a tool for hydrogeology (2nd ed., pp. 347–366). Springer. doi:10.1007/978-3-540-88405-7_12

Dinwiddie CL, Molz FJ, Castle JW (2003) A new small drill hole minipermeameter probe for in situ permeability measurement: Fluid mechanics and geometrical factors. Water Resources Research 39(7): 1–13. doi:10.1029/2001WR001179

Dinwiddie CL, Bradbury KK, McGinnis RN, Fedors RW, Ferrill DA (2006) Fault zone deformation overprints permeability of nonwelded ignimbrite: Chalk Cove Fault, Bishop Tuff, Bishop, California. Vadose Zone Journal 5: 610–627. doi:10.2136/vzj2005.0062

Dinwiddie CL, Bradbury KK, McGinnis RN, Stillman DE, Ferrill DA (2012) Hydrogeologic heterogeneity of faulted and fractured Glass Mountain bedded tuffaceous sediments and ash-fall deposits: The Crucifix site near Bishop, California. Lithosphere, January: 1–23. doi:10.1130/L179.1

Dlubac K, Knight R, Song Y-Q, Bachman N, Grau B, Cannia J, Williams J (2013) Use of NMR logging to obtain estimates of hydraulic conductivity in the High Plains aquifer, Nebraska, USA. Water Resour. Res. 49: 1871–1886. doi:10.1002/wrcr.20151

Freeze AR, Cherry JA (1979) Groundwater. Prentice Hall Inc., New Jersey, 604 p.

Gedeon M, Mallants D (2009) Hydrogeological modelling in support of site characterisation. NIROND-TR 2008-36 E, NIRAS-MP5-03 DATA-LT(HYD), April 2009. Available from www.researchgate.net/publication/27412843, last accessed on 22/01/2014.

Gedeon M, Mallants D, Rogiers B (2013) Building a staircase of confidence in groundwater modeling: a summary of ten years data collection and model development. Proceedings of MODFLOW and More 2013: Translating Science into Practice. Golden, Colorado, 2-5 June 2013, 6 pp.

Goggin DJ, Chandler MA, Korcurek GA, Lake LW (1988a) Patterns of permeability in eolian deposits: Page Sandstone (Jurassic), northeastern Arizona. SPE Formation Eval. 3: 297-306

Goggin DJ, Thrasher RL, Lake LW (1988b) A theoretical and experimental analysis of minipermeameter response including gas slippage and high velocity flow effects. In Situ 12: 79-116

Goovaerts P (1997) Geostatistics for natural resources evaluation (Applied Geostatistics Series) (p. 496). Oxford University Press, USA.

Goss D, Zlotnik VA (2007) Air permeameter investigation of surficial dune structures in the Nebraska Sand Hills. AAPG Bull. 91(5): 645–652. doi:10.1306/11200606009

Halvorsen C, Hurst A (1990) Principles, practice, and applications of laboratory minipermeametry, in: Advances in core evaluation: accuracy and precision in reserves estimation, edited by: Worthington PF, Gordon and Breach, London, 521–549

Huysmans M, Dassargues A (2005) Stochastic analysis of the effect of heterogeneity and fractures on radionuclide transport in a low permeability clay layer. Enviromental Geology 48(7): 920-930

Huysmans M, Peeters L, Moermans G, Dassargues A (2008) Relating small-scale sedimentary structures and permeability in a cross-bedded aquifer. J Hydrology 361(1-2): 41-51

Huysmans M, Dassargues A (2009) Application of multiple-point geostatistics on modelling groundwater flow and transport in a cross-bedded aquifer (Belgium). Hydrogeology J, 17(8): 1901–1911

Huysmans M, Dassargues A (2011) Direct multiple-point geostatistical simulation of edge properties for modeling thin irregularly shaped surfaces. Mathematical Geosciences 43(5): 521–536. doi:10.1007/s11004-011-9336-7

Iversen BV, Moldrup P, Schjonning P, Jacobsen OH (2003) Field application of a portable air permeameter to characterize spatial variability in air and water permeability. Vadose Zone J 2(4): 618-626

Jensen JL, Glasbey CA, Corbett PWM (1994) On the interaction of geology, measurement, and statistical-analysis of small-scale permeability measurements. Terra Nova 6(4): 397–403

Jiang Z, Schrank C, Mariethoz G, Cox M (2013) Permeability estimation conditioned to geophysical downhole log data in sandstones of the northern Galilee Basin, Queensland: Methods and application. J Appl Geophysics. doi:10.1016/j.jappgeo.2013.03.008

Kirkham D (1947) Field method for determination of air permeability of soil in its undisturbed state. Soil Sci Soc Am Proc 11:93–99

Klute A (1965) Laboratory measurement of hydraulic conductivity of saturate soil. In: Methods of soil analysis, part 1, physical and mineralogical methods. Agron. Monogr. 9, American Society of Agronomy, Madison, WI.

Loll P, Moldrup P, Schjønning P, Riley H (1999) Predicting saturated hydraulic conductivity from air permeability: Application in stochastic water infiltration modeling. Water Resour Res 35(8): 2387–2400

Mallants D, Labat S, Gedeon M (2003) Bijkomende sitekarakterisatie voor de nucleaire zone Mol-Dessel : bepaling van de hydrogeologische parameters. SCK•CEN-R-3703 (p. 82). Mol, Belgium

McKinley JM, Lloyd CD, Ruffell AH (2004) Use of variography in permeability characterisation of visually homogeneous sandstone reservoirs with examples from outcrop studies. Mathematical Geology 36: 761–779

McKinley JM, Atkinson PM, Lloyd CD, Ruffell AH, Worden RH (2011) How porosity and permeability vary spatially with grain size, sorting, cement volume, and mineral dissolution in fluvial Triassic sandstones: The value of geostatistics and local regression. J Sedimentary Res 81: 844–858

McLean RA, Sanders WL, Stroup WW (1991) A unified approach to mixed linear models. The American Statistician 45(1): 54–64

Molz FJ, Dinwiddie CL, Wilson JL (2003) A physical basis for calculating instrument spatial weighting functions in homogeneous systems. Water Resources Research 39(4): 1-14. doi:10.1029/2001WR001220

New England Research, Vindum Engineering (2011) TinyPerm II portable air permeameter, user’s manual. Retrieved from http://www.vindum.com/TinyPermManual.pdf on 14-06-2011

Nilsson B, Højberg A, Refsgaard J, Troldborg L (2007) Uncertainty in geological and hydrogeological data. Hydrology and Earth Syst Sciences 11: 1551-1561

ONDRAF/NIRAS (2010) Het cAt-project in Dessel. Een langetermijnoplossing voor het Belgische categorie A-afval. Retrieved from http://www.niras-cat.be/downloads/cAt_masterplan_NL_LOW.pdf on 07-12-2011

Pebesma EJ (2004) Multivariable geostatistics in S: the gstat package. Computers & Geosciences 30: 683-691

Possemiers M, Huysmans M, Peeters L, Batelaan O, Dassargues A (2012) Relationship between sedimentary features and permeability at different scales in the Brussels Sands. Geologica Belgica 15(3): 156-164

Rasmussen TC, Evans DD, Sheets PJ, Blanford EH (1993) Permeability of Apache Leap Tuff: Borehole and core measurements using water and air. Water Resour Res 29(7): 1997–2006

R Development Core Team (2012) R: A language and environment for statistical computing. R foundation for statistical computing, Vienna, Austria. ISBN 3-900051-07-0, URL http://www.R-project.org/

Robertson GM, McPhee CA (1990) High-resolution probe permeability: An aid to reservoir description, in: Advances in core evaluation, volume 1: accuracy and precision in reserves estimation, edited by: Worthington PF, Gordon and Breach, London, 495–520

Rogiers B, Mallants D, Batelaan O, Gedeon M, Huysmans M, Dassargues A (2012) Estimation of hydraulic conductivity and its uncertainty from grain-size data using GLUE and artificial neural networks. Mathematical Geosciences 44(6): 739–763

Rogiers B, Beerten K, Smeekens T, Mallants D, Gedeon M, Huysmans M, Batelaan O, Dassargues A (2013a) Derivation of flow and transport parameters from outcropping sediments of the Neogene aquifer, Belgium. Geologica Belgica 16(3): 129-147

Rogiers B, Beerten K, Smeekens T, Mallants D, Gedeon M, Huysmans M, Batelaan O, Dassargues A (2013b) The usefulness of outcrop analogue air permeameter measurements for analysing aquifer heterogeneity: Quantifying outcrop hydraulic conductivity and its spatial variability. Hydrological processes, available online. doi: 10.1002/hyp.10007

Rogiers B, Beerten K, Smeekens T, Mallants D, Gedeon M, Huysmans M, Batelaan O, Dassargues A (2013c) The usefulness of outcrop analogue air permeameter measurements for analysing aquifer heterogeneity: testing outcrop hydrogeological parameters with independent borehole data. Hydrol Earth Syst Sci 17: 5155-5166

Rogiers B, Vienken T, Gedeon M, Batelaan O, Mallants D, Huysmans M, Dassargues A (2014) Multi-scale aquifer characterization and groundwater flow model parameterization using direct push technologies. Environmental Earth Sciences, submitted.

Ronayne MJ, Gorelick SM, Zheng C (2010) Geological modeling of submeter scale heterogeneity and its influence on tracer transport in a fluvial aquifer. Water Resour Res 46(10): 1-9

Sheskin DJ (2004) Handbook of parametric and nonparametric statistical procedures. Third edition. Chapman & Hall/CRC. ISBN 1-58488-440-1

Shipton ZK, Evans JP, Robeson KR, Forster CB, Snelgrove S (2002) Structural heterogeneity and permeability in faulted eolian sandstone: Implications for subsurface modeling of faults. AAPG Bulletin 86(5): 863–883

Slater L (2007) Near surface electrical characterization of hydraulic conductivity: From petrophysical properties to aquifer geometries - a review. Surveys in Geophysics, 169–197. doi:10.1007/s10712-007-9022-y

Tartakovsky DM, Moulton JD, Zlotnik VA (2000) Kinematic structure of minipermeameter flow. Water Resources Research 36(9): 2433–2442. doi:10.1029/2000WR900178

Thomas CJS (1998) Reservoir characterization of a shallow marine sandstone: the Lower Cretaceous Sandringham Sands (Leziate Beds) and Carstone formations, eastern England. Petroleum Geoscience 4(3): 215-219

Welby CW (1981) A technique for evaluating the hydraulic conductivity of saprolite. UNC-WRRI-81-164

Wemaere I, Marivoet J, Labat S, Beaufays R, Maes T (2002) Mol-1 borehole (April-May 1997) – Core manipulations and determination of hydraulic conductivities in the laboratory. Report R-3590, SCK•CEN, Mol, Belgium

Wemaere I, Marivoet J, Labat S (2008) Hydraulic conductivity variability of the Boom Clay in north-east Belgium based on four core drilled boreholes. Physics and Chemistry of the Earth 33: S24-S36. doi:10.1016/j.pce.2008.10.051

Yu L, Rogiers B, Gedeon M, Marivoet J, De Craen M, Mallants D (2013) A critical review of laboratory and in-situ hydraulic conductivity measurements for the Boom Clay in Belgium. Appl. Clay Science 75-76: 1-12

Figure captions

Figure 1: Map of the study area location within Western Europe (a), and detailed map of the study area, with the location of the Nuclear zone and studied boreholes (b).

Figure 2: Core sampling and preparation for air permeability measurements: Schematic of separation of the core slab from the main core (a); longitudinal sawing of the core with a wire saw (b); 100 cm³ steel ring core sampling for hydraulic conductivity determination in the lab (c); and the execution of hand-held air permeameter measurements on the core slabs (d).

Figure 3: Typical borehole cores of the different lithostratigraphical units (from shallowest to deepest sediments): Quaternary (a); Mol Upper Sands (b); Mol Lower Sands (c); Kasterlee Sands (d); Kasterlee Clay (e); Diest Clayey Top (f); and Diest Sands (g).

Figure 4: Scatterplots of K_h versus K_v derived from laboratory measurements of the 100 cm³ steel ring core samples for: (a) the upper aquifer units Quaternary (Q), Mol Upper (MU) and Lower (ML), and Kasterlee Sands (KS); (b) the Kasterlee Clay aquitard; (c) the lower aquifer units Diest Clayey Top (DCT) and the Diest Sands (DS).

Figure 5: Overview of all raw data (100 cm³ lab-based K_s and k_a-based $K_{s,ap}$ values obtained with the equation of Loll *et al.* (1999)) for two examples out of the seven studied boreholes (Dessel-3 and Dessel-4).

Figure 6: Boxplots of median, first and third quartile, and 95% confidence interval K_s values from K_h laboratory analysis (a), K_v laboratory analyses (b), and $K_{s,ap}$ data (c), based on Loll et al. (1999), for each of the stratigraphical units. The whiskers extend to the most extreme data point which is no more than 1.5 times the interquartile range from the box; the data points beyond that (outliers) are plotted individually. The number of observations is provided each time as well.

Figure 7: Effect of gravimetric water content on $K_{s,ap}$ using full-sized core samples. The highest water content represents the condition after unpacking of the cores (i.e. removal of the vacuum seal), the second point is water content after a week of drying in open air, and the final (i.e. zero) water content is obtained after 48 hrs drying in an oven at 100°C. The individual samples (displayed transparantly) are grouped, and the group means are provided for cores near grain size data with clay contents > 10 % (clay), < 10% and > 2.5% (clayey sand), and < 2.5 % (sand).

Figure 8: Scatterplot of the uncalibrated air permeameter $K_{s,ap}$ values using Loll *et al.* (1999) versus laboratory K_s (a), and calibrated $K_{s,ap}$ data by means of linear mixed effects models for K_h and K_v, with a random effect for the lithostratigraphy and borehole factors (b).

Figure 9: Experimental direct variogram and cross-variograms of the standardized data, for K_h (a) and K_v (b). The corresponding variogram models consist of a short (0.4 m) and long range (12 m) spherical variogram model.

Figure 10: Vertical profiles of lab-based K_h values, the calibrated air permeameter-based K_h estimates ($K_{h,ap}$), and the co-kriging estimates and their 95% confidence interval for two examples out of the seven studied boreholes: Dessel-3 (a) and Dessel-4 (b).

Figure 11: Overview of the primary K_h and K_v data together with the corresponding co-kriging estimates for two examples out of the seven studied boreholes: Dessel-3 (a) and Dessel-4 (b). The K_h data is the same as that presented in Figure 10.

Figure 12: Leave-one-out cross-validation results for inverse distance weighting (a), ordinary kriging (b), and ordinary co-kriging (c). R^2 is provided on the figures, other performance measures can be found in Table 2.

Figure 1

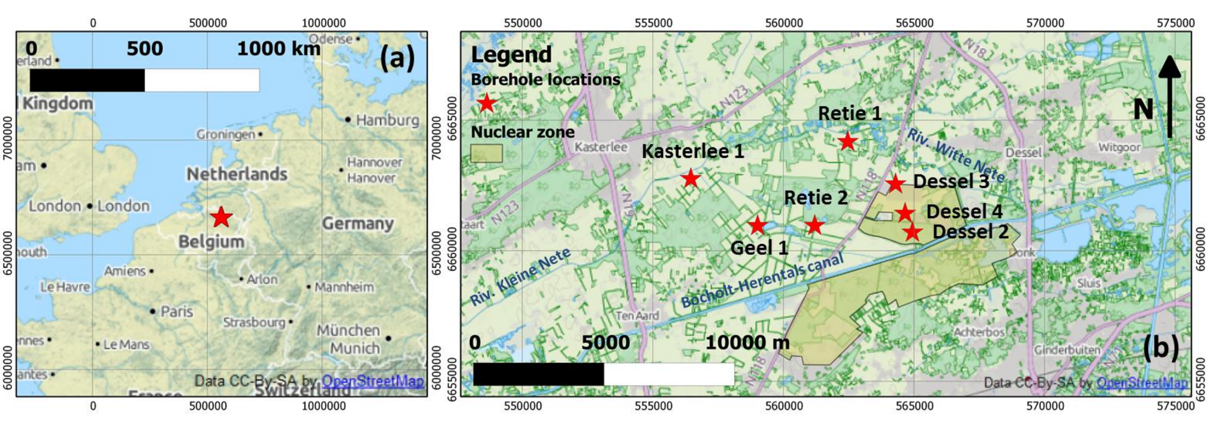

0
500
1000 km
(a)
Kingdom
Netherlands
Germany
Belgium
London
Groningen
Hamburg
Hannover
Hanover
Amiens
Le Havre
Paris
Arlon
Mannheim
Strasbourg
München
Munich
Le Mans
Data CC-By-SA by OpenStreetMap
Legend
Borehole locations
Nuclear zone
Retie 1
Kasterlee 1
Retie 2
Geel 1
Dessel 3
Dessel 4
Dessel 2
Riv. Witte Nete
Riv. Kleine Nete
Bocholt-Herentals canal
Kasterlee
Dessel
Witgoor
Ten Aard
Achterbos
Sluis
Ginderbuiten
N
0
5000
10000 m
(b)
Data CC-By-SA by OpenStreetMap

Figure 2

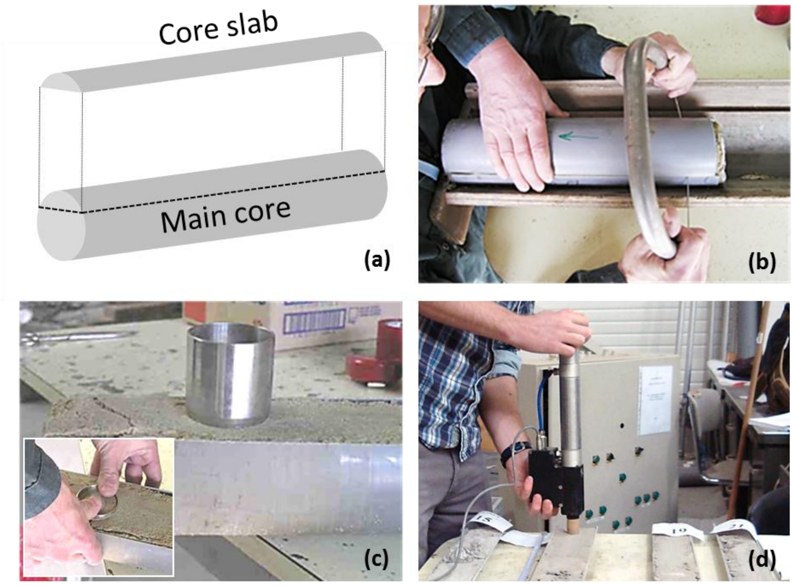

Figure 3

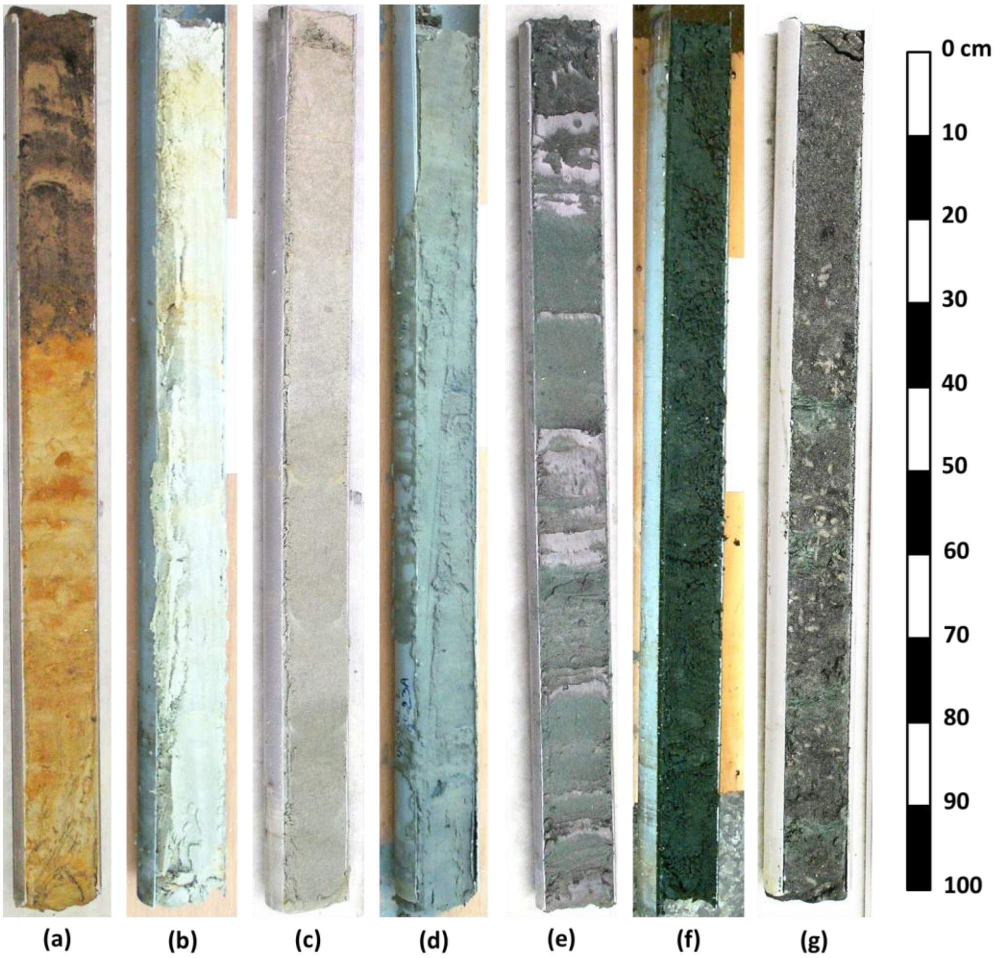

Figure 4

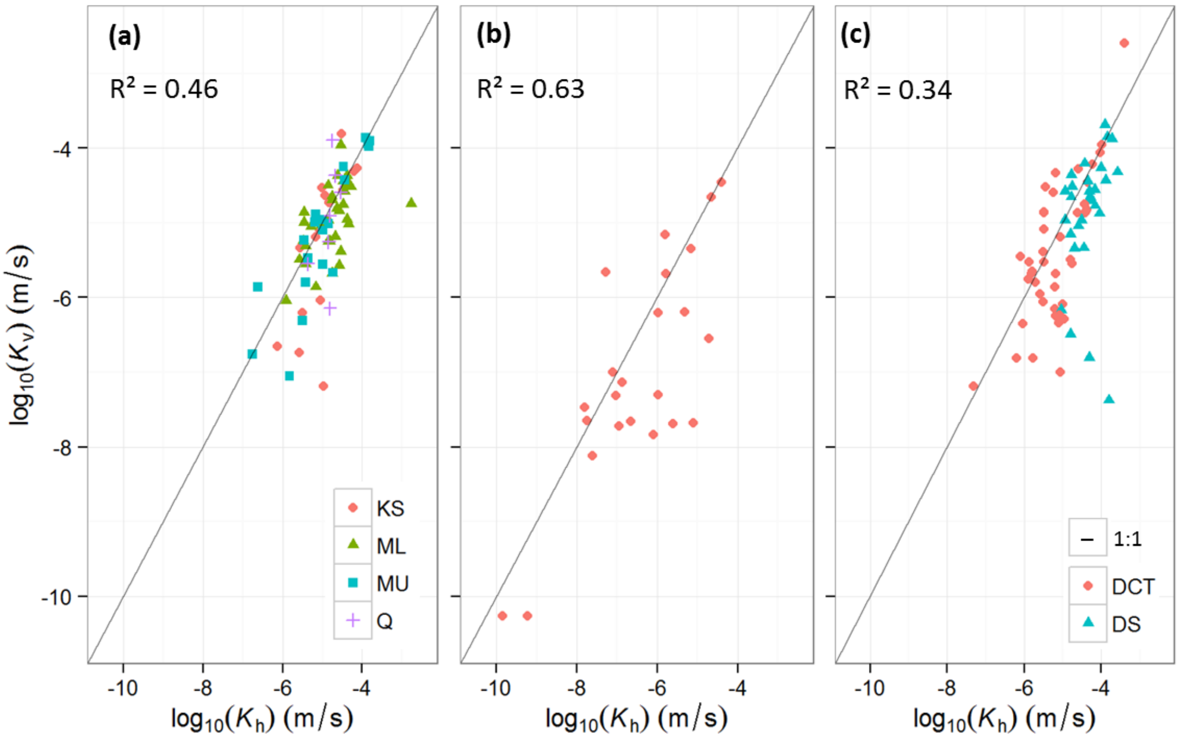

(a)
R² = 0.46
(b)
R² = 0.63
(c)
R² = 0.34
-4
-6
-8
-10
log10(Kv) (m/s)
-10
-8
-6
-4
log10(Kh) (m/s)
KS
ML
MU
Q
1:1
DCT
DS

Figure 5

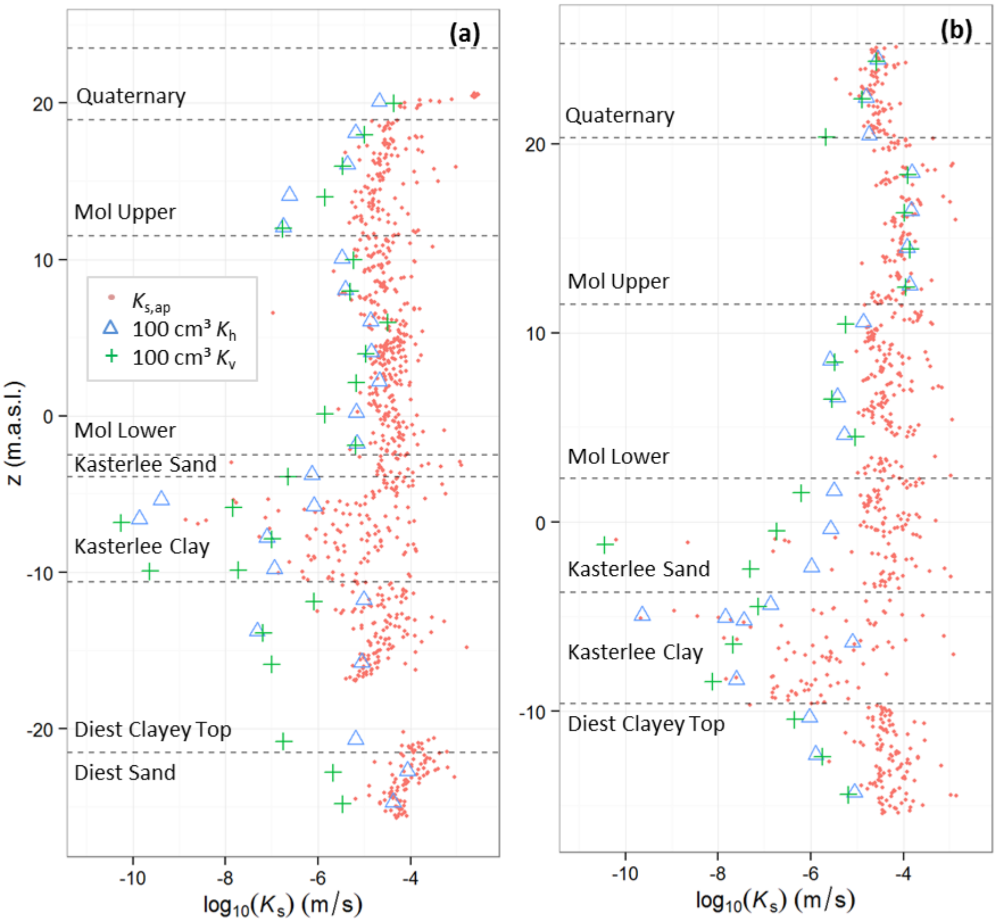

(a)
(b)
Quaternary
Mol Upper
Mol Lower
Kasterlee Sand
Kasterlee Clay
Diest Clayey Top
Diest Sand
$K_{s,ap}$
100 cm³ K_h
100 cm³ K_v
z (m.a.s.l.)
$\log_{10}(K_s)$ (m/s)
20
10
0
-10
-20
-10
-8
-6
-4

Figure 6

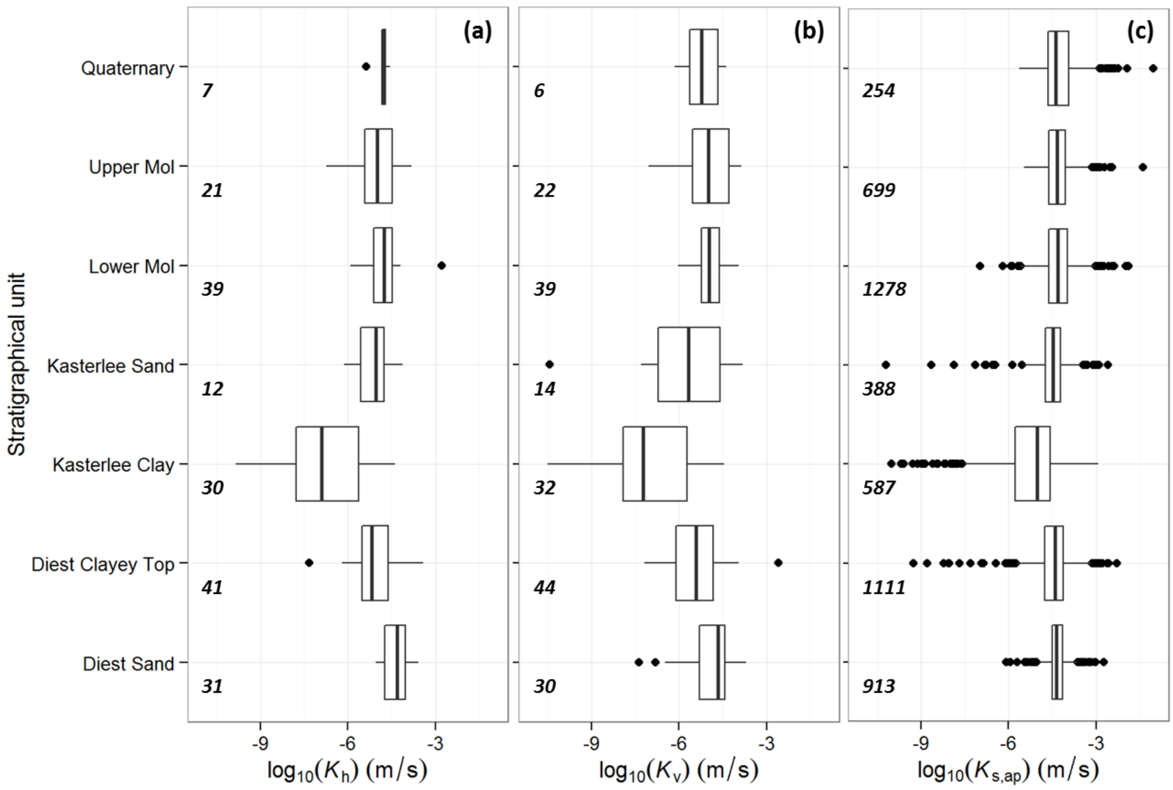

(a)
(b)
(c)
Stratigraphical unit
Quaternary
Upper Mol
Lower Mol
Kasterlee Sand
Kasterlee Clay
Diest Clayey Top
Diest Sand
7
21
39
12
30
41
31
6
22
39
14
32
44
30
254
699
1278
388
587
1111
913
-9
-6
-3
log10(Kh) (m/s)
log10(Kv) (m/s)
log10(Ks,ap) (m/s)

Figure 7

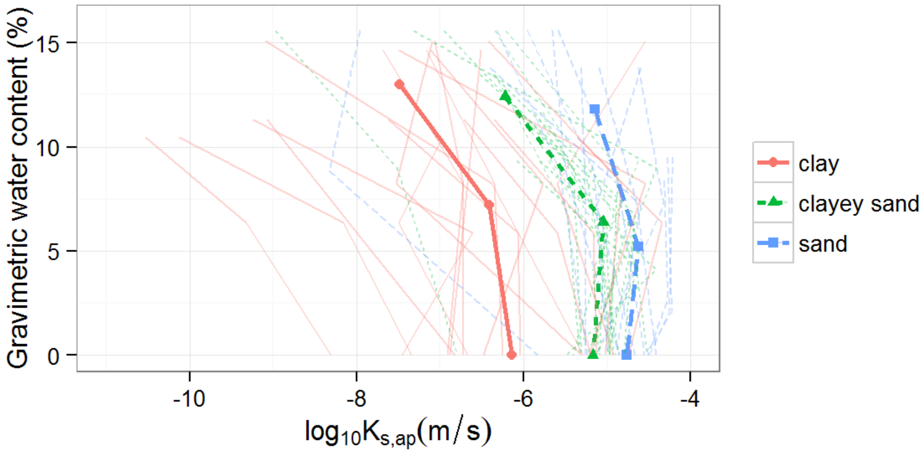

Gravimetric water content (%)
15
10
5
0
-10
-8
-6
-4
log10Ks,ap(m/s)
clay
clayey sand
sand

Figure 8

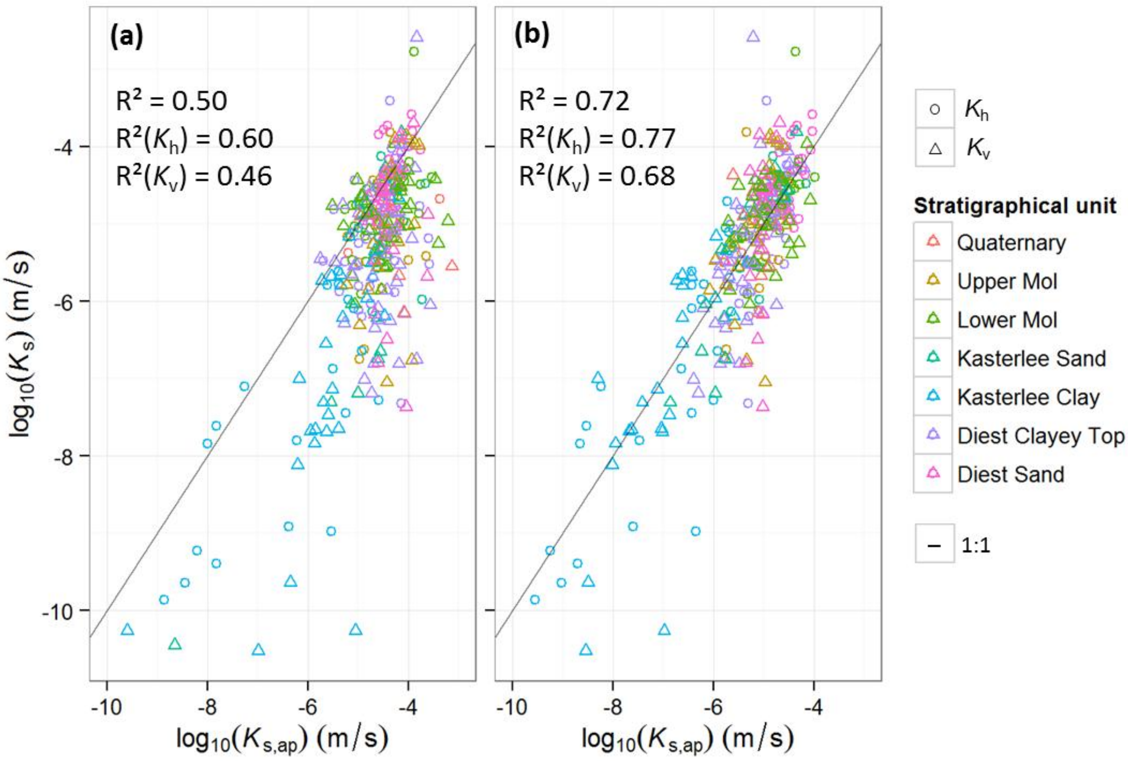

(a)
R^2 = 0.50
$R^2(K_h)$ = 0.60
$R^2(K_v)$ = 0.46
(b)
R^2 = 0.72
$R^2(K_h)$ = 0.77
$R^2(K_v)$ = 0.68
$\log_{10}(K_s)$ (m/s)
$\log_{10}(K_{s,ap})$ (m/s)
-4
-6
-8
-10
K_h
K_v
Stratigraphical unit
Quaternary
Upper Mol
Lower Mol
Kasterlee Sand
Kasterlee Clay
Diest Clayey Top
Diest Sand
1:1

Figure 9

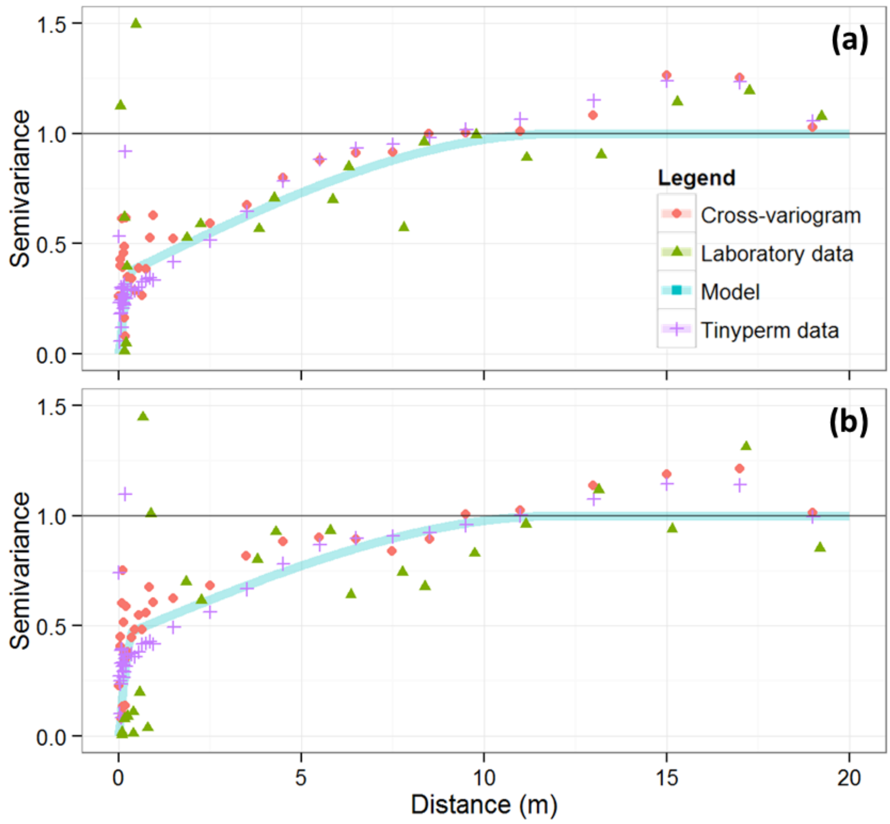

(a)
(b)
Semivariance
Semivariance
1.5
1.0
0.5
0.0
Legend
Cross-variogram
Laboratory data
Model
Tinyperm data
0
5
10
15
20
Distance (m)

Figure 10

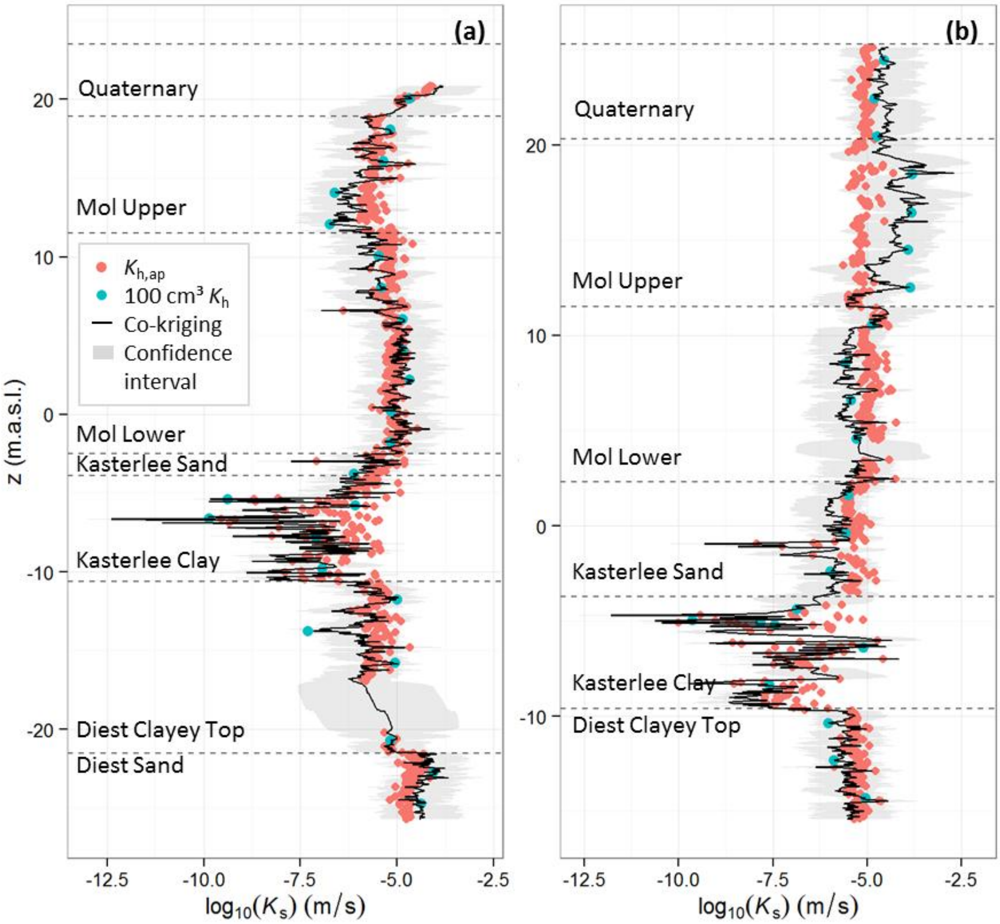

(a)
Quaternary
Mol Upper
Mol Lower
Kasterlee Sand
Kasterlee Clay
Diest Clayey Top
Diest Sand
$K_{h,ap}$
100 cm³ K_h
Co-kriging
Confidence interval
z (m.a.s.l.)
$\log_{10}(K_s)$ (m/s)
(b)
Quaternary
Mol Upper
Mol Lower
Kasterlee Sand
Kasterlee Clay
Diest Clayey Top
$\log_{10}(K_s)$ (m/s)

Figure 11

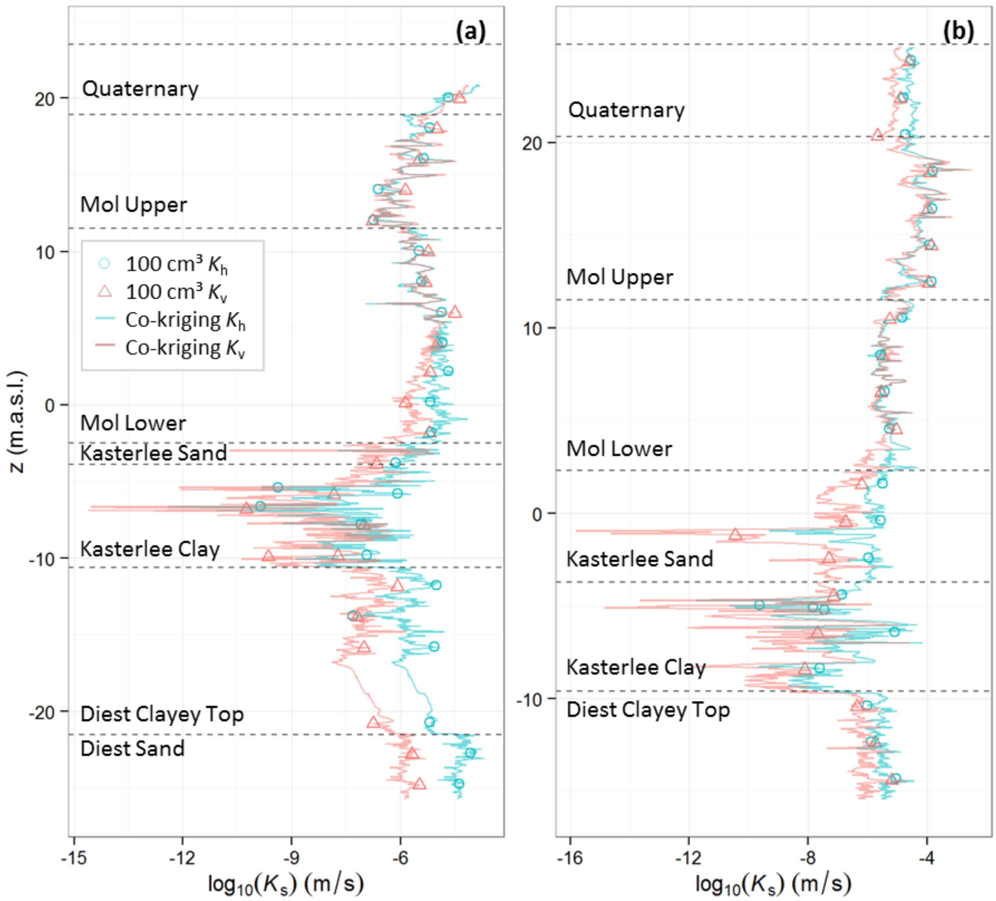
(a)
(b)
Quaternary
Mol Upper
Mol Lower
Kasterlee Sand
Kasterlee Clay
Diest Clayey Top
Diest Sand
100 cm³ K_h
100 cm³ K_v
Co-kriging K_h
Co-kriging K_v
z (m.a.s.l.)
$\log_{10}(K_s)$ (m/s)
20
10
0
-10
-20
-15
-12
-9
-6
-16
-8
-4

Figure 12

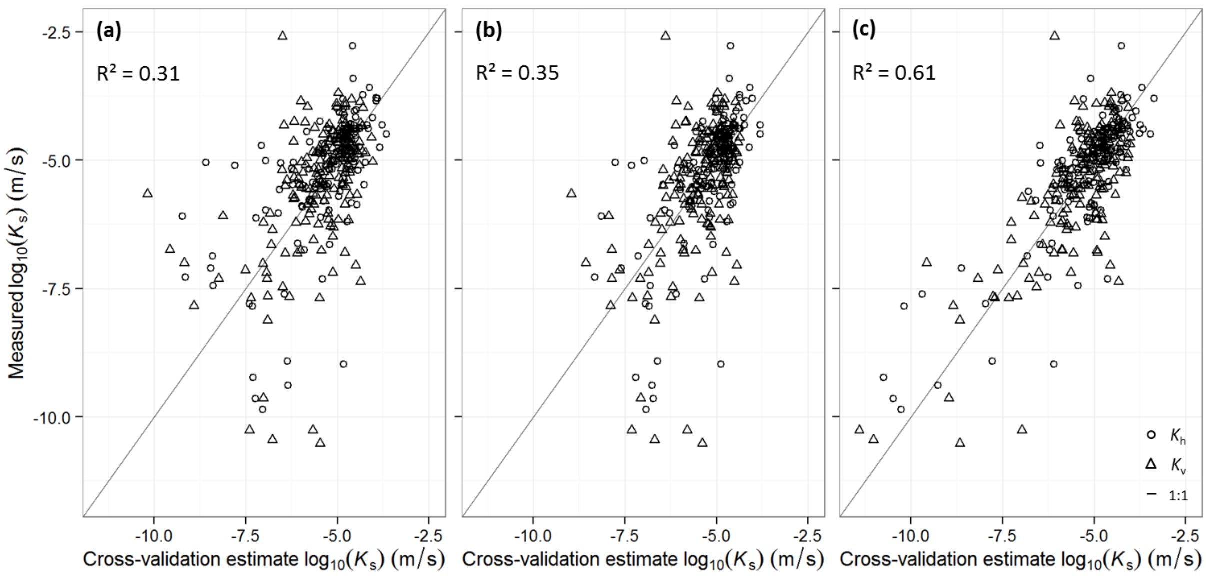

(a)
R² = 0.31
(b)
R² = 0.35
(c)
R² = 0.61
Measured log10(Ks) (m/s)
Cross-validation estimate log10(Ks) (m/s)
-2.5
-5.0
-7.5
-10.0
Kh
Kv
1:1